



**HAL**  
open science

## Ferromagnetic L 10 phase formation in the Mn–Al–C alloys induced by high-pressure spark plasma sintering

Muriel Tyrman, Simon Quetel-Weben, Alexandre Pasko, Loic Perriere, Ivan Guillot, Victor H. Etgens, Frédéric Mazaleyrat

### ► To cite this version:

Muriel Tyrman, Simon Quetel-Weben, Alexandre Pasko, Loic Perriere, Ivan Guillot, et al.. Ferromagnetic L 10 phase formation in the Mn–Al–C alloys induced by high-pressure spark plasma sintering. *IEEE Transactions on Magnetics*, 2017, 53, pp.2101505. 10.1109/TMAG.2017.2732500 . hal-01489975

**HAL Id: hal-01489975**

**<https://hal.science/hal-01489975>**

Submitted on 14 Mar 2017

**HAL** is a multi-disciplinary open access archive for the deposit and dissemination of scientific research documents, whether they are published or not. The documents may come from teaching and research institutions in France or abroad, or from public or private research centers.

L'archive ouverte pluridisciplinaire **HAL**, est destinée au dépôt et à la diffusion de documents scientifiques de niveau recherche, publiés ou non, émanant des établissements d'enseignement et de recherche français ou étrangers, des laboratoires publics ou privés.

# Ferromagnetic $L_{10}$ phase formation in the Mn–Al–C alloys induced by high-pressure spark plasma sintering

Muriel Tyrman<sup>1,2</sup>, Simon Quétel-Weben<sup>3</sup>, Alexandre Pasko<sup>1</sup>, Loïc Perrière<sup>3</sup>,  
Ivan Guillot<sup>3</sup>, Victor Etgens<sup>2</sup>, and Frédéric Mazaleyrat<sup>1</sup>, *Member, IEEE*

<sup>1</sup>SATIE, ENS Cachan, CNRS, Université Paris-Saclay, Cachan, France

<sup>2</sup>LISV, Université de Versailles Saint-Quentin-en-Yvelines, Velizy, France

<sup>3</sup>ICMPE, CNRS, Université Paris-Est Creteil, Thiais, France

Structural and magnetic characterization of Mn–Al–C permanent magnets obtained by spark plasma sintering (SPS) is reported. The transformation from the parent  $\epsilon$ -phase to the ferromagnetic  $\tau$ -phase occurs simultaneously with the process of sintering. The use of a tungsten carbide crucible enabled us to decrease the sintering temperature, which hampered the precipitation of secondary phases. As a result, the sintered samples show higher coercivity as compared to the annealed powder. However, the finely milled powder, ensuring better densification, turned out to be more prone to phase decomposition during sintering. The phase constitution of the samples was determined by X-ray diffraction, magnetic hysteresis loops were recorded using a vibrating sample magnetometer. Scanning electron microscopy and electron backscatter diffraction were employed to study the microstructure and orientation distribution of grains after SPS. The dependence of coercivity and magnetization on the preparation conditions and sintering temperature is analyzed. To combine good magnetic properties with proper density, further optimization of the production parameters is necessary.

*Index Terms*—Permanent magnets, manganese-aluminum alloys, magnetic properties, spark plasma sintering.

## I. INTRODUCTION

THE tetragonal  $\tau$ -phase in the Mn–Al system belongs to the prominent family of ferromagnetic alloys with  $L_{10}$  ordered crystal structure. In recent years this material has received a new attention as a promising candidate for permanent magnet applications [1], [2], [3], [4], [5], [6], [7], between inexpensive hard ferrites and high-performance Nd–Fe–B magnets. The Mn–Al alloy is light, does not contain any rare-earth elements and can be used, for example, in the automotive industry. However, the  $\tau$ -phase is metastable and therefore needs an optimization of its production route. Moreover, the relatively low values of coercivity attained so far, as compared to a good anisotropy field of about 5 T [8], [9], suggest the necessity of the microstructure optimization.

The  $\tau$ -phase is usually obtained in the  $Mn_{50+x}Al_{50-x}$  composition ( $x = 0 \dots 10$ , atom %) by quenching the high-temperature hexagonal  $\epsilon$ -phase with subsequent heat treatment at 400 to 700 °C, during which the  $\epsilon \rightarrow \tau$  structural phase transformation occurs. To avoid the decomposition into a pair of equilibrium phases, a small quantity of carbon is added, which also improves the coercivity [10]. Recently, we proposed to employ the spark plasma sintering (SPS) method in order to combine the synthesis step (formation of the  $\tau$ -phase) and sintering step (creation of solid material, potentially anisotropic, from powder) [2], [9]. However, the optimal thermal conditions of synthesis and sintering turn out to be not the same. They depend on the relative stabilities of the phases involved, the diffusion rates, etc. Note that the SPS technique has another variable parameter which significantly affects the process: uniaxial pressure, applied (unlike in conventional sintering) simultaneously with heat. Therefore, here we present the results of structural and magnetic investigations of the Mn–

Al–C magnetic materials obtained by sintering the powder precursors at elevated pressure.

## II. EXPERIMENTAL

The ternary alloys with nominal composition  $Mn_{54}Al_{44}C_2$  were prepared as follows. Pure manganese, aluminum and  $Mn_{23}C_6$  compound were melted in a cold crucible induction furnace. The  $\epsilon$ -phase ribbons produced by melt-spinning were comminuted using two methods: hand-grinding and cryogenic mechanical milling, which give different particle size distributions. Then the obtained powders were sintered in 8 mm tungsten carbide molds by electric current direct heating under argon, or just annealed in a furnace for comparison. The tungsten carbide molds allow application of much higher pressure than the graphite ones that we used before [2], [9]. This in turn ensured a good densification of pellets at lower sintering temperatures. The obtained powder and solid samples were characterized using the X-ray diffraction (XRD), vibrating sample magnetometry (VSM), scanning electron microscopy (SEM) and electron backscatter diffraction (EBSD). The measurements were performed using a Bruker D2 Phaser diffractometer equipped with a LinxEye linear detector in Co  $K\alpha$  radiation, a Lake Shore 7400 magnetometer, and a Zeiss Merlin microscope equipped with a field emission gun.

## III. RESULTS AND DISCUSSION

The preparation conditions (fine or coarse milling, temperature of annealing or sintering) and corresponding sample labels are presented in Table I. The density of sintered samples was measured by the Archimedes method. The relative density, calculated using the XRD data and also shown in Table I, is higher for fine milling and increases with increase of heat treatment temperature.

TABLE I  
PREPARATION CONDITIONS AND RELATIVE DENSITY OF SAMPLES.

Sample	Form	Granularity	Treatment (°C)	Density (%)
PF550	Powder	Fine	550	–
SF500	Bulk	Fine	500	95
SF550	Bulk	Fine	550	99
SC500	Bulk	Coarse	500	92
SC550	Bulk	Coarse	550	95
SC600	Bulk	Coarse	600	100

TABLE II  
PHASE FRACTIONS AND CRYSTALLITE SIZE DETERMINED BY XRD.

Sample	$\tau$ -phase (%)	$\gamma_2$ -phase (%)	$\beta$ -phase (%)	Grains (nm)
PF550	64	–	36	101
SF500	75	–	25	67
SF550	66	5	29	59
SC500	100	–	–	54
SC550	93	–	7	56
SC600	90	–	10	70

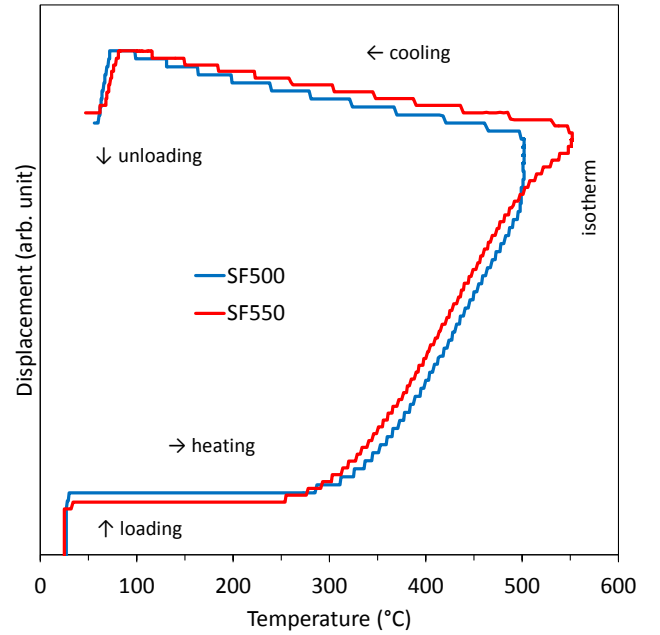
Typical behavior of the  $\text{Mn}_{54}\text{Al}_{44}\text{C}_2$  materials during sintering is shown in Fig. 1 which depicts the displacement of the die (due to sample shrinkage) under a pressure of 400 MPa as a function of temperature. The heating/cooling rate is 100 K/min with an isothermal pause of 5 min. It is seen that the powder densification starts at 300 to 400 °C depending on the granularity and finishes at about 550 °C. If the sintering is incomplete on heating, it continues at the plateau corresponding to the maximum temperature.

According to the Al-Mn phase diagram, for the chosen composition two equilibrium phases are expected to form: the Mn-rich cubic  $\beta$ -phase and the Al-rich trigonal  $\gamma_2$ -phase. In addition, two metastable phases may appear in non-equilibrium conditions: the hexagonal  $\epsilon$ -phase and the tetragonal  $\tau$ -phase. Stable at higher temperatures, the  $\epsilon$ -phase can be preserved on quenching and transformed into the ferromagnetic  $\tau$ -phase by a composition-invariant structural transition.

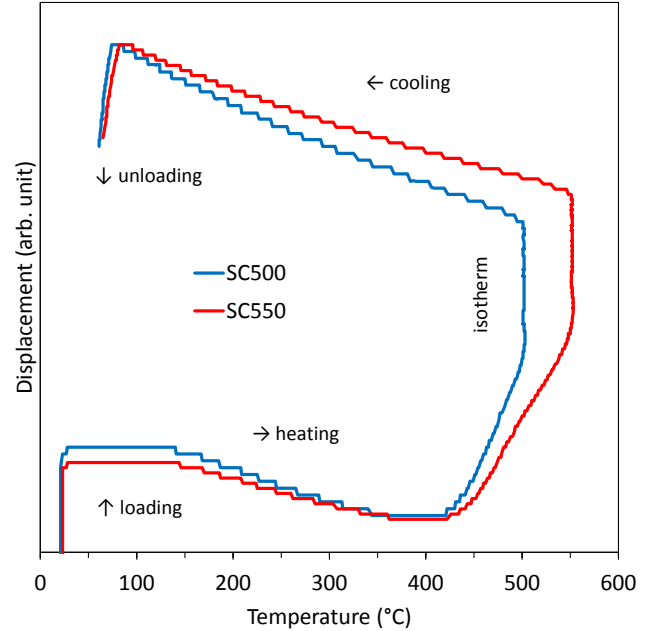
The phase constitutions of powder and solid samples were determined by the XRD quantitative analysis using the Rietveld refinement software MAUD (and confirmed by VSM measurements). We found that the cryogenically milled powder is more prone to decomposition into stable non-magnetic phases during annealing or sintering than the hand-ground one (probably, because of mechanical activation), therefore the milling regime should be chosen carefully. The decrease of the sintering temperature also influences favorably the ferromagnetic  $\tau$ -phase volume fraction, important for maximizing the saturation magnetization.

XRD patterns of the sintered samples are shown in Fig. 2, the phase fractions and coherently scattering domain size determined from the profile fitting are presented in Table II.

Typical magnetization loops of the  $\text{Mn}_{54}\text{Al}_{44}\text{C}_2$  powder and solid samples are shown in Fig. 3a. Note the significant increase of coercivity from 0.17 T for the furnace-annealed at 550 °C powder to 0.26 T for the sintered at 500 °C and 400 MPa pellet. This in some degree unexpected result (as



(a)

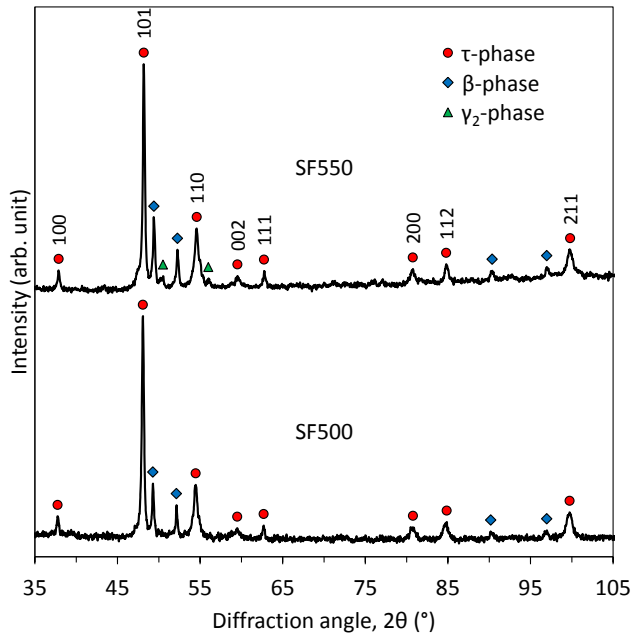


(b)

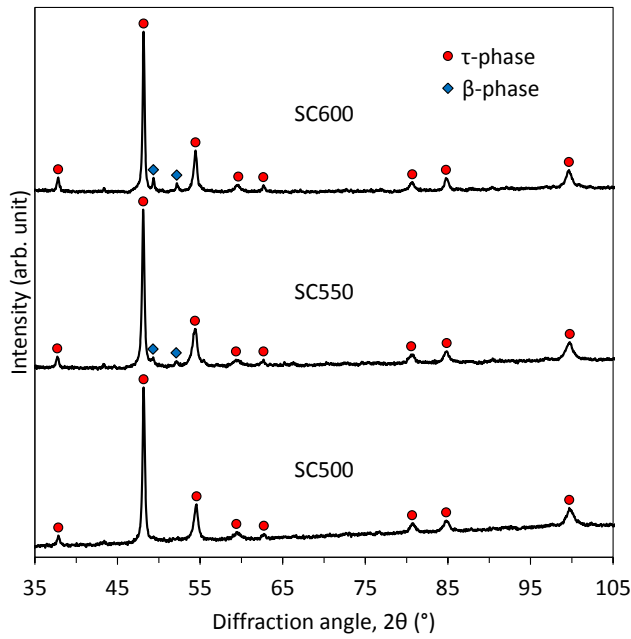
Fig. 1. Deformation of the  $\text{Mn}_{54}\text{Al}_{44}\text{C}_2$  samples under pressure as a function of temperature during sintering: (a) fine milling, (b) coarse milling.

usually the coercivity decreases after sintering with increase of density and ferromagnetic phase fraction [2]) confirms that by choosing the proper regimes of milling and sintering one can improve the magnetic properties of Mn–Al–C alloys. The complex microstructure of these materials, resulted from the processes of structural transformation and grain growth stimulated by applied heat and pressure, directly affects their magnetization behavior.

When measuring the magnetic properties of the sintered



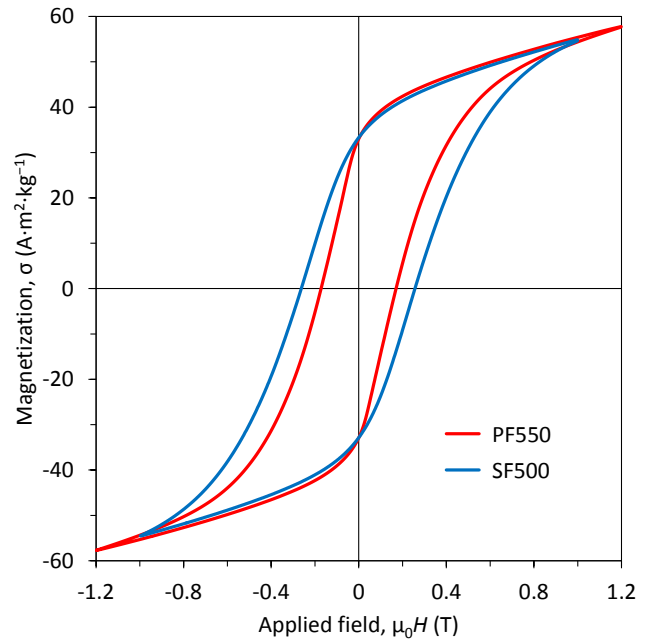
(a)



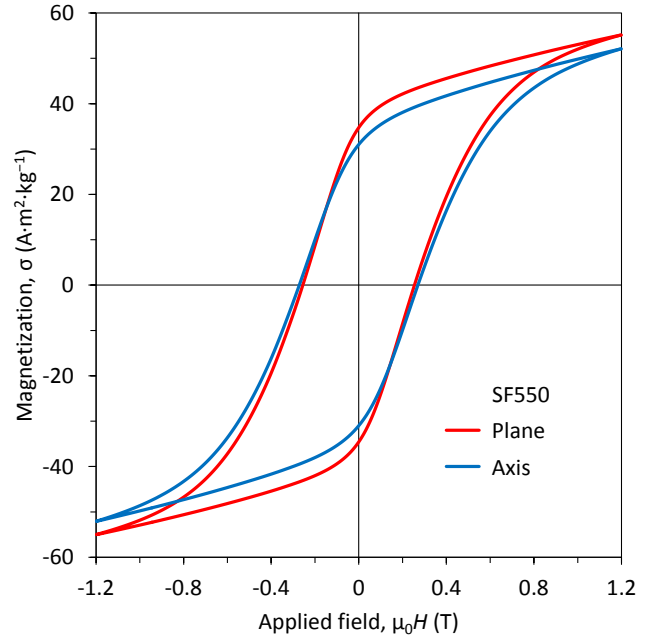
(b)

Fig. 2. XRD patterns of the sintered  $\text{Mn}_{54}\text{Al}_{44}\text{C}_2$  samples (Co  $K\alpha$  radiation): (a) fine milling, (b) coarse milling.

samples, we noticed some anisotropy induced by the uniaxial pressure applied during SPS. As shown in Fig. 3b, magnetization is higher when the field is perpendicular to the direction of pressure (plane), whereas coercivity is slightly higher when the field is parallel to it (axis). The magnetic properties (coercivity, magnetization at maximum field, remanence, and maximum energy product) of the samples determined for these two orientations are presented in Table III. We can see in particular that coercivity is higher for fine milling and it increases with



(a)



(b)

Fig. 3. Magnetization loops of the  $\text{Mn}_{54}\text{Al}_{44}\text{C}_2$  samples, fine milling: (a) annealed powder and sintered material, (b) magnetic field is applied parallel and perpendicular to the direction of sintering pressure.

sintering temperature. However, coarse milling delivers higher concentration of the ferromagnetic phase.

Microstructure and crystalline texture of the sintered samples were studied by and EBSD. Fig. 4a presents the orientation distribution of the  $\tau$ -phase and  $\beta$ -phase grains, whereas Fig. 4b shows the phase map. We can see that the  $\beta$ -phase grains decorate large groups of the  $\tau$ -phase grains. These groups possibly correspond to former particles (grains) of the  $\epsilon$ -phase powder which partitioned after the  $\epsilon \rightarrow \tau$  structural

TABLE III  
COERCIVITY  $\mu_0 H_c$ , SATURATION MAGNETIZATION  $J_s$ , REMANENCE  $J_r$ ,  
AND MAXIMUM ENERGY PRODUCT  $(BH)_{max}$ .

Sample	Orientation	$\mu_0 H_c$ (mT)	$J_s$ (mT)	$J_r$ (mT)	$(BH)_{max}$ (kJ·m <sup>-3</sup> )
PF550	–	171	–	–	–
SF500		246	352	202	5.3
SF500	⊥	232	379	226	6.1
SF550		271	332	197	5.3
SF550	⊥	255	351	220	6.1
SC500		186	418	194	4.3
SC500	⊥	177	434	209	4.6
SC550		192	444	226	5.4
SC550	⊥	177	466	245	5.7
SC600		203	451	245	6.4
SC600	⊥	187	476	266	6.6

transformation. In this case the  $\beta$ -phase grains can appear at the boundaries of the former particles with higher concentration of defects and nuclei. The pole figures of the  $\tau$ -phase orientation distributions determined from EBSD is shown in Fig. 5. The crystalline texture seems to be near isotropic.

#### IV. CONCLUSION

Bulk Mn<sub>54</sub>Al<sub>44</sub>C<sub>2</sub> permanent magnets were produced by spark plasma sintering of the precursors obtained using rapid solidification and ball milling. The increase of applied pressure allowed us to decrease the sintering temperature, which influenced positively the volume fraction of the ferromagnetic  $\tau$ -phase. In order to improve the material density, finely milled powder was prepared. As a result, the sintered samples show higher coercivity as compared to the annealed powder. A small anisotropy of magnetic properties, induced by the sintering pressure, was observed. However, ball milling, by increasing surface area and introducing defects, facilitates the decomposition of the  $\epsilon$ -phase powder into equilibrium phases. Therefore, the choice of powder granularity and sintering parameters (pressure and temperature) needs further optimization.

#### ACKNOWLEDGMENT

M. T. thanks MATINNOV Chair for funding her PhD thesis.

#### REFERENCES

- [1] J. M. D. Coey, "New permanent magnets; manganese compounds," *J. Phys. Condens. Matter*, vol. 26, p. 064211, Feb. 2014.
- [2] A. Pasko, M. LoBue, E. Fazakas, L. K. Varga, and F. Mazaleyrat, "Spark plasma sintering of Mn-Al-C hard magnets," *J. Phys. Condens. Matter*, vol. 26, p. 064203, Feb. 2014.
- [3] P. Saravanan, V. T. P. Vinod, M. Černik, A. Selvapriya, D. Chakravarty, and S. V. Kamat, "Processing of Mn-Al nanostructured magnets by spark plasma sintering and subsequent rapid thermal annealing," *J. Magn. Mater.*, vol. 374, pp. 427–432, Jan. 2015.
- [4] R. Madugundo and G. C. Hadjipanayis, "Anisotropic Mn-Al(C) hot-deformed bulk magnets," *J. Appl. Phys.*, vol. 119, p. 013904, Jan. 2016.
- [5] L. G. Marshall, I. J. McDonald, and L. H. Lewis, "Quantification of the strain-induced promotion of  $\tau$ -MnAl via cryogenic milling," *J. Magn. Mater.*, vol. 404, pp. 215–220, Apr. 2016.
- [6] H. Fang, S. Kontos, J. Ångström, J. Cedervall, P. Svedlindh, K. Gunnarsson, and M. Sahlberg, "Directly obtained  $\tau$ -phase MnAl, a high performance magnetic material for permanent magnets," *J. Solid State Chem.*, vol. 237, pp. 300–306, May 2016.
- [7] W. Lu, J. Niu, T. Wang, K. Xia, Z. Xiang, Y. Song, H. Zhang, S. Yoshimura, and H. Saito, "Low-energy mechanically milled  $\tau$ -phase MnAl alloys with high coercivity and magnetization," *J. Alloy. Compd.*, vol. 675, pp. 163–167, Aug. 2016.
- [8] L. Pareti, F. Bolzoni, F. Leccabue, and A. E. Ermakov, "Magnetic anisotropy of MnAl and MnAlC permanent magnet materials," *J. Appl. Phys.*, vol. 59, pp. 3824–3828, Jun. 1986.
- [9] A. Pasko, F. Mazaleyrat, L. K. Varga, P. Stamenov, and J. M. D. Coey, "High-field magnetization behavior of Mn-Al-C alloys," *IEEE Trans. Magn.*, vol. 50, p. 2105104, Nov. 2014.
- [10] T. Ohtani, N. Kato, S. Kojima, K. Kojima, Y. Sakamoto, I. Konno, M. Tsukahara, and T. Kubo, "Magnetic properties of Mn-Al-C permanent magnet alloys," *IEEE Trans. Magn.*, vol. 13, pp. 1328–1330, 1977.

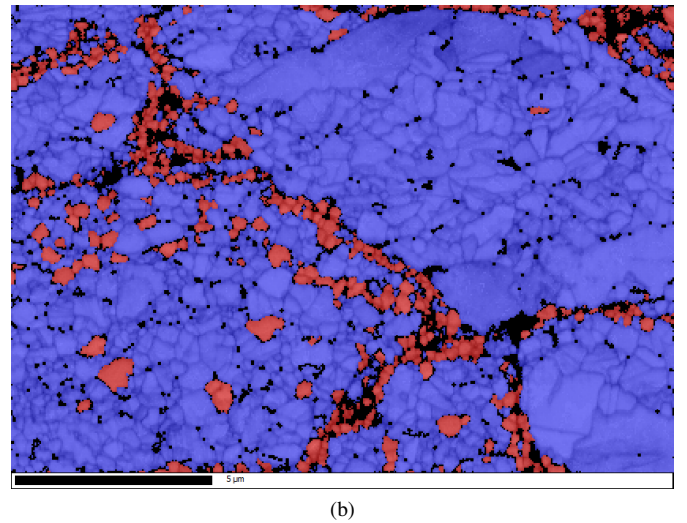
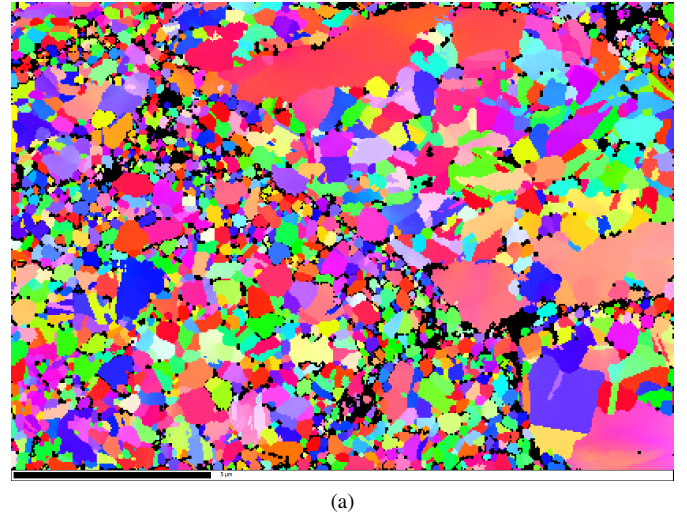


Fig. 4. EBSD images of the SF500 sample microstructure: (a) orientation distribution of grains, (b)  $\tau$ -phase grains are blue,  $\beta$ -phase grains are red.

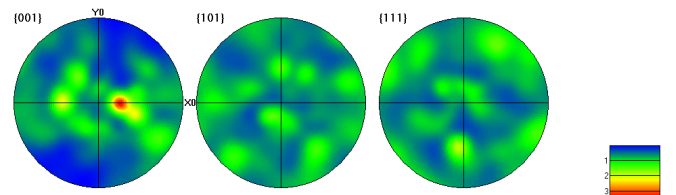


Fig. 5. EBSD pole figures of the  $\tau$ -phase orientation distribution.